Int. J. Solids Structures Vol. 25, No. 10, pp. 1177–1191, 1989
Printed in Great Britain

0020–7683/89 $3.00 + .00

SCATTERING OF FLEXURAL WAVES BY CAVITIES IN A PLATE

R. PASKARAMOORTHY and A. H. SHAH
Department of Civil Engineering, University of Manitoba, Winnipeg, Manitoba, Canada R3T 2N2

and

S. K. DATTA
Department of Mechanical Engineering and CIRES, University of Colorado, Boulder, CO 80309, U.S.A.

(*Received* 13 *January* 1988; *in revised form* 20 *December* 1988)

Abstract—In this paper, the scattering of slow flexural waves by arbitrary shaped cavities in an infinite elastic plate is studied using a combined finite element and analytical method. The problem is considered as consisting of two interacting systems, a bounded interior region containing all material and geometric irregularities, and an unbounded exterior region. The interior region is modelled by using Mindlin type plate bending elements. Wave function expansion is used to represent the exterior region. Continuity of displacements and tractions are enforced at the nodes on the finite element interface with the exterior region. Comparison of present results for circular cavity with the analytical solution shows excellent agreement. Finally, scattering by triangular and square shaped cavities as well as a pair of circular cavities is considered.

INTRODUCTION

In an isotropic, infinite elastic medium, two types of waves (P and S) propagate, but in a plate in flexure entirely different types of waves propagate. The scattering by an obstacle of an elastic wave propagating in an infinite medium has been widely studied by Pao and Mow (1973). However, except for the contribution of Pao and Chao (1964), no other study has been reported on the scattering problem of flexural waves in a plate.

Three types of waves can propagate in an isotropic elastic plate in flexure based on Mindlin theory; slow flexural, fast flexural and thickness shear waves. Pao and Chao (1964) studied the scattering of slow flexural waves in an isotropic infinite elastic plate by the wave function expansion method. In their treatment, both the incident and scattered fields are expanded in Fourier Bessel series. For a cylindrical inclusion having circular cross-section, they evaluated the scattered wave field by satisfying the boundary conditions prescribed over the surface of the inclusion. However, the boundary conditions for a scatterer having arbitrary cross-section cannot be satisfied which is the limitation of the analytical approach.

The method of wave function expansion has also been used to study scattering of elastic waves in two- and three-dimensional problems. Pao and Mow (1973) give a comprehensive coverage of this subject. The limitation of this method, as noted above, is its inability to satisfy the boundary conditions over the scatterer–host medium interface when the scatterer has arbitrary cross-section.

Problems involving arbitrary geometric configurations are more ammenable to numerical methods such as finite elements and finite differences. An obvious shortcoming of such schemes is that the domain, which is usually infinite for the class of problems under consideration, has to be modelled by a finite-sized model. Attempts have been made (Lysmer and Kuhlemeyer, 1969; Smith, 1974; Kausel *et al.*, 1975; Chow and Smith, 1981; Medina and Taylor, 1983; Lee and Dasgupta, 1984) to reduce the error stemming from the use of finite-sized model by prescribing appropriate boundary conditions to be used along the boundary of the finite computational domain. By and large, they are either approximate in nature or work best at certain angles of incidence. Similar attempts for transient wave propagation has been reported (Engquist and Majda, 1977; Higden, 1986, 1987). Recently Ting and Miksis (1986) proposed a scheme to generate the exact boundary data but a numerical implementation and a comparison of accuracy of their scheme is yet to be reported.

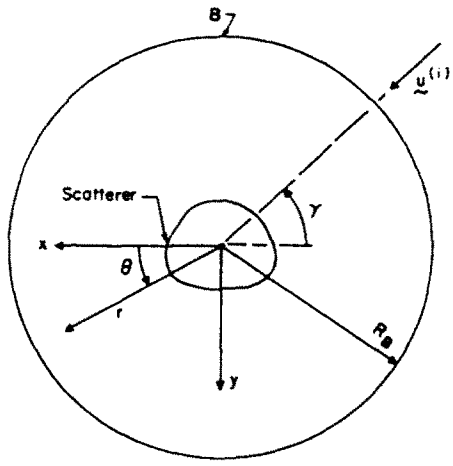

Fig. 1. Geometry of the problem.

The present authors used a numerical technique combining the wave function expansion procedure with the finite element method to study this class of problems. The success of this technique has been reported earlier (Shah *et al.*, 1982a,b; Datta *et al.*, 1982; Datta and Shah, 1982; Abduljabbar *et al.*, 1983; Shah *et al.*, 1985; Shah *et al.*, 1987; Paskaramoorthy *et al.*, 1988). In these studies, the general strategy was to draw a fictitious boundary B (Fig. 1) enclosing the scatterer. The region interior to this boundary (referred to as "interior region" in the following) which consists of the scatterer and a finite region of host medium was modelled through an assemblage of conventional finite elements. The solution in the exterior region was represented by wave function expansion. Imposing continuity conditions for displacements and traction forces at the nodal points on B, the unknown coefficients associated with the scattered waves in the exterior region and the displacements at the boundary nodes were obtained. They were then used to calculate the field at any point outside B as well as the nodal displacements in the interior region. The technique has the advantage that the scatterer can be quite arbitrary in shape and in material properties. Also the multiple scattering by a cluster of scatterers can be studied. In essence, this numerical technique, which exploits the great flexibility of finite elements in modelling complicated geometries and boundary conditions, relies on wave functions to capture the far-field behaviour. Research is now underway to extend this technique to analyse problems where explicit wave functions are not available.

In this paper, we use this numerical technique to study the scattering of flexural waves by a cylindrical scatterer (or a cluster of scatterers) in an isotropic infinite elastic plate. The interior region is modelled by Mindlin type plate bending elements. The exterior region is represented by flexural wave functions. The cross-section of the scatterer can be arbitrary, but for illustration purposes we only consider circle, triangle and square shape cavities. The case of multiple scattering by two right circular cylindrical cavities is also considered. The plate is excited by time harmonic slow flexural wave that is incident obliquely making an angle γ to the x-axis. (Fig. 1). Numerical results are presented for various normalized frequencies in the range 0.1–0.9, the normalization factor being $p_0 = \pi C_2/h$ in which h is the plate thickness and C_2 is the shear wave velocity in an infinite elastic medium. Note that the normalization factor for frequencies is the lowest circular frequency of the simple thickness shear modes of a plate based on the three dimensional theory.

FORMULATION OF THE PROBLEM

(a) *Finite element model of interior region*

The details of the formulation of Mindlin type plate bending elements have been discussed by Cook (1981) and Hughes *et al.* (1977), so that there is no need for repeating them here. Only the relevant details will be given to underscore the discussion.

In Mindlin's theory for flexural vibration of plates, the displacement components, when referred to Cartesian coordinates, are assumed as

$$u_x = z\psi_x(x, y)\, e^{-ipt}$$
$$u_y = z\psi_y(x, y)\, e^{-ipt}$$
$$u_z = w(x, y)\, e^{-ipt}. \tag{1}$$

Thus the displacement at any point is completely defined by the components of the generalized displacement vector $\{\mathbf{W}\}$, where

$$\{\mathbf{W}\} = \langle w\psi_x\psi_y\rangle^T \tag{2}$$

in which w is the lateral displacement, ψ_x and ψ_y are rotations in the xz and yz planes, respectively.

In eqn (1), a steady state time variation of e^{-ipt} is assumed (p-circular frequency). This occurs throughout and may be omitted for notational convenience.

The generalized displacement vector $\{\delta\}$ at a point within an element e is interpolated from the nodal values as

$$\{\mathbf{W}\} = [N^e(x, y)]\{\mathbf{q}^e\} \tag{3}$$

where $[N^e(x, y)]$ contains the interpolation functions, $\{\mathbf{q}^e\}$ is the vector of nodal variables for element e.

The bending moments $\{M\}$ and shear force $\{Q\}$ are related to the generalized strain components $\{\varepsilon_b\}$ and $\{\varepsilon_s\}$ by the expressions

$$\{M\} = [D_b]\{\varepsilon_b\} \tag{4}$$

$$\{Q\} = [D_s]\{\varepsilon_s\} \tag{5}$$

where

$$\{M\} = \langle M_x M_y M_{xy}\rangle^T \tag{6}$$

$$\{Q\} = \langle Q_x Q_y\rangle^T \tag{7}$$

$$\{\varepsilon_b\} = \left\langle \frac{\partial\psi_x}{\partial x}, \frac{\partial\psi_y}{\partial y}, \left(\frac{\partial\psi_x}{\partial y} + \frac{\partial\psi_y}{\partial x}\right)\right\rangle^T \tag{8}$$

$$\{\varepsilon_s\} = \left\langle \frac{\partial w}{\partial x} + \psi_x, \frac{\partial w}{\partial y} + \psi_y\right\rangle^T \tag{9}$$

$$[D_b] = \frac{Eh^3}{12(1-\nu)^2}\begin{bmatrix} 1 & \nu & 0 \\ \nu & 1 & 0 \\ 0 & 0 & \dfrac{1-\nu}{2} \end{bmatrix} \tag{10}$$

$$[D_s] = \frac{Eh\kappa^2}{2(1+\nu)}\begin{bmatrix} 1 & 0 \\ 0 & 1 \end{bmatrix}. \tag{11}$$

In the above, E is the Young's modulus, h the thickness, ν the Poisson's ratio and κ^2 the shear correction factor. Note that we use the Mindlin's value of $\pi^2/12$ for the shear correction factor instead of the conventional Reissner's value of 5/6. The Lagrangian of the system

can be written as

$$L = \frac{1}{2}\int (\mathbf{M}\cdot\boldsymbol{\varepsilon}_b^* + \mathbf{Q}\cdot\boldsymbol{\varepsilon}_s^* - p^2\mathbf{W}^T\mathbf{P}\mathbf{W}^*)\,\mathrm{d}x\,\mathrm{d}y - \frac{1}{2}\int_B (\mathbf{F}_B\cdot\mathbf{W}_B^* + \mathbf{F}_B^*\cdot\mathbf{W}_B)\,\mathrm{d}s \tag{12}$$

where (*) indicates complex conjugate, $\mathbf{F}_B$ and $\mathbf{W}_B$ are, respectively, the generalized traction and displacement vectors on the boundary B, and $[P]$ is the inertia matrix which is given as

$$[P] = \rho\begin{bmatrix} h & 0 & 0 \\ 0 & h^3/12 & 0 \\ 0 & 0 & h^3/12 \end{bmatrix} \tag{13}$$

in which ρ is the mass density per unit volume. The governing equations of motion of the system can be obtained by minimizing the eqn (12) and expressed as

$$[S]\{\mathbf{q}\} = \{\mathbf{R}\} \tag{14}$$

where

$$[S] = [K] - p^2[M] \tag{15}$$

in which $[K]$ and $[M]$ are, respectively, the global stiffness and mass matrices of the interior region, $\{\mathbf{q}\}$ is the vector of nodal variables and $\{\mathbf{R}\}$ is the vector of generalized loads which has non-zero components corresponding to the interface degrees of freedom only. Note that the boundary B is a fictitious circle of radius R_B, which is arbitrary.

If the vector $\{\mathbf{q}\}$ of nodal variables is separated into two parts, $\{\mathbf{q}_B\}$ corresponding to the nodal variables at the boundary B and $\{\mathbf{q}_I\}$ corresponding to the nodal variables elsewhere in the interior region, eqn (14) can be written as

$$\begin{bmatrix} S_{II} & S_{IB} \\ S_{BI} & S_{BB} \end{bmatrix}\begin{bmatrix} \mathbf{q}_I \\ \mathbf{q}_B \end{bmatrix} = \begin{bmatrix} 0 \\ \mathbf{R}_B \end{bmatrix}. \tag{16}$$

(b) *Flexural wave functions for exterior region (scattered field)*

In the exterior region, the total displacement $\mathbf{u}$, which consists of the incident wave field component $\mathbf{u}^{(i)}$ and scattered wave field component $\mathbf{u}^{(s)}$, can be written, in cylindrical coordinates system, as

$$\begin{aligned} u_r &= z\psi_r(r,\theta) \\ u_\theta &= z\psi_\theta(r,\theta) \\ u_z &= w(r,\theta). \end{aligned} \tag{17}$$

The steady state time factor e^{-ipt} is omitted in the foregoing equations and hereafter when its existence is apparent. The generalized displacement components w, ψ_r and ψ_θ may be expressed in terms of three potentials W_1, W_2 and H, as given by Mindlin and Deresiewicz (1954),

$$W = W_1 + W_2 \tag{18a}$$

$$\psi_r = (\sigma_1 - 1)\frac{\partial W_1}{\partial r} + (\sigma_2 - 1)\frac{\partial W_2}{\partial r} + \frac{1}{r}\frac{\partial H}{\partial \theta} \tag{18b}$$

$$\psi_\theta = (\sigma_1 - 1)\frac{1}{r}\frac{\partial W_1}{\partial \theta} + (\sigma_2 - 1)\frac{1}{r}\frac{\partial W_2}{\partial \theta} - \frac{\partial H}{\partial r} \tag{18c}$$

where the three potentials satisfy

$$(\nabla^2+\delta_1^2)W_1 = 0 \tag{19a}$$

$$(\nabla^2+\delta_2^2)W_2 = 0 \tag{19b}$$

$$(\nabla^2+\omega^2)H = 0. \tag{19c}$$

In the foregoing equations

$$\delta_1^2, \delta_2^2 = \tfrac{1}{2}\delta_0^4\{(R+S)\pm\sqrt{(R-S)^2+4\delta_0^{-4}}\} \tag{20a}$$

$$\langle\sigma_1, \sigma_2\rangle^T = (R\delta_0^4 - S^{-1})^{-1}\langle\delta_2^2\delta_1^2\rangle^T \tag{20b}$$

$$\omega^2 = 2(R\delta_0^4 - S^{-1})/(1-\nu) \tag{20c}$$

$$R = h^2/12, \quad S = D/\kappa^2 Gh, \quad \delta_0^4 = \rho p^2 h/D \tag{20d}$$

where h is the thickness of the plate, ν the Poisson's ratio, D the flexural rigidity and G the shear modulus. The wave number δ_1 is always real. For frequencies $p < p_0$, both the wave numbers δ_2 and ω are imaginary. The scattered wave field satisfying eqn (19) can be written as

$$W_1 = \sum\{A_{1n}H_n(\delta_1 r)\cos n\theta + A_{2n}H_n(\delta_1 r)\sin n\theta\} \tag{21a}$$

$$W_2 = \sum\{B_{1n}K_n(\delta_2 r)\cos n\theta + B_{2n}K_n(\delta_2 r)\sin n\theta\} \tag{21b}$$

$$H = \sum\{C_{1n}K_n(\bar{\omega}r)\sin n\theta + C_{2n}K_n(\bar{\omega}r)\cos n\theta\} \tag{21c}$$

where the constants A_{1n}, B_{1n} and C_{1n} corresponds to a symmetric problem and A_{2n}, B_{2n} and C_{2n} corresponds to an anti-symmetric problem.

$$\delta_2^2 = -\delta_2^2, \quad \bar{\omega}^2 = -\omega^2. \tag{22}$$

H_n is the Hankel function of the first kind and K_n the modified Bessel function of the second kind. The summation goes from zero to infinity through integer values of n. Note that the eqn (21) represents a wave field that radiates outward from the origin. Substituting eqn (21) and eqn (18), we get

$$w = \sum\{[A_{1n}g_1 + B_{1n}g_2]\cos n\theta + [A_{2n}g_1 + B_{2n}g_2]\sin n\theta\}$$

$$\psi_r = \sum\{[A_{1n}g_{r1} + B_{1n}g_{r2} + C_{1n}g_{r3}]\cos n\theta + [A_{2n}g_{r1} + B_{2n}g_{r2} - C_{2n}g_{r3}]\sin n\theta\}$$

$$\psi_\theta = \sum\{[A_{1n}g_{t1} + B_{1n}g_{t2} + C_{1n}g_{t3}]\sin n\theta + [-A_{2n}g_{t1} - B_{2n}g_{t2} + C_{2n}g_{t3}]\cos n\theta\}. \tag{23}$$

Expressions for g_1, g_2, etc. are presented in the Appendix. Evaluating eqns (23a–c) at each of the nodes lying on the boundary B, the vector $\{\mathbf{q}_B^{(s)}\}$ of nodal variables due to scattered field can be written as

$$\{\mathbf{q}_B^{(s)}\}_{cyl} = [G]\{\mathbf{a}\} \tag{24}$$

where $\{\mathbf{q}_B^{(s)}\}_{cyl}$ contains the nodal variables, in cylindrical coordinate system, evaluated at the nodes on the boundary B, $\{\mathbf{a}\}$ contains the unknown coefficients A_{1n}, B_{1n}, etc. In writing eqn (24), the summation of the terms containing the coefficients A_{1n}, B_{1n} and C_{2n} is taken from zero to $((N_B/2)-1)$ where N_B is the number of nodes on the boundary. The summation of A_{2n}, B_{2n} and C_{1n} goes from one to $N_B/2$. Thus $[G]$ is a square matrix.

The vector $\{\mathbf{q}_B^{(s)}\}_{cyl}$ in eqn (24) can be transformed into Cartesian coordinate system

as

$$\{\mathbf{q}_B^{(s)}\} = [T][G]\{\mathbf{a}\} \tag{25}$$

where $[T]$ is the transformation matrix.

The next step is to construct the boundary nodal force vector corresponding to the generalized displacement vector $\{\mathbf{q}_B^{(s)}\}$. It should be noted here that the components of the force vector $\{\mathbf{R}_B^{(s)}\}$ corresponding to the displacements w, ψ_x and ψ_y at the boundary B are Q_r, $(M_{rr}l_1 - M_{r\theta}l_2)$ and $(M_{rr}l_2 + M_{r\theta}l_1)$, respectively, where l_1 $(= \cos\theta)$ and l_2 $(= \sin\theta)$ are the direction cosines of the normal to the boundary B.

The stress resultants for the displacement field in eqn (23) can be expressed as

$$Q_r = \kappa^2 Gh \sum \{[A_{1n}Q_{r1} + B_{1n}Q_{r2} + C_{1n}Q_{r3}] \cos n\theta + [A_{2n}Q_{r1} + B_{2n}Q_{r2} - C_{2n}Q_{r3}] \sin n\theta\} \tag{26a}$$

$$M_{rr} = D \sum \{[A_{1n}M_{r1} + B_{1n}M_{r2} + C_{1n}M_{r3}] \cos n\theta + [A_{2n}M_{r1} + B_{2n}M_{r2} - C_{2n}M_{r3}] \sin n\theta\} \tag{26b}$$

$$M_{r\theta} = \frac{D}{2}(1-\nu) \sum [A_{1n}M_{rt1} + B_{1n}M_{rt2} + C_{1n}M_{rt3}] \sin n\theta + [-A_{2n}M_{rt1} - B_{2n}M_{rt2} + C_{2n}M_{rt3}] \cos n\theta. \tag{26c}$$

Expressions for Q_{r1}, Q_{r2}, etc. are given in the Appendix. Evaluating the stress resultants at each of the nodes lying on the boundary B and multiplying by the tributary area, the boundary nodal force vector can now be assembled as

$$\{\mathbf{R}_B^{(s)}\} = [F]\{\mathbf{a}\}. \tag{27}$$

As the number of ns considered in writing eqn (27) is the same as that for eqn (24), the $[F]$ matrix is of the same size as $[G]$ and square and non-singular. Eliminating $\{\mathbf{a}\}$ from eqns (25) and (27), we get

$$\{\mathbf{R}_B^{(s)}\} = [S_f]\{\mathbf{q}_B^{(s)}\} \tag{28a}$$

where

$$[S_f] = [F][G]^{-1}[T]^{-1}. \tag{28b}$$

The impedance matrix $[S_f]$ is square and complex-valued but unsymmetric.

(c) *Incident wave field*

The incident slow flexural wave propagating in a direction making an angle γ with the x-axis can be represented by

$$W_1^{(i)} = e^{ik_1(x\cos\gamma + y\sin\gamma)}, \quad W_2^{(i)} = H^{(i)} = 0. \tag{29}$$

For this incident field, the displacements and stress resultants can be derived and the vectors $\{\mathbf{q}_B^{(i)}\}$ and $\{\mathbf{R}_B^{(i)}\}$ corresponding to $\{\mathbf{q}_B^{(s)}\}$ and $\{\mathbf{R}_B^{(s)}\}$ can be constructed in a similar manner.

(d) *Global solution*

The continuity conditions of displacements and traction forces at the boundary nodes are

$$\mathbf{q}_B = \mathbf{q}_B^{(i)} + \mathbf{q}_B^{(s)} \tag{30a}$$

$$\mathbf{R}_B = \mathbf{R}_B^{(i)} + \mathbf{R}_B^{(s)}. \tag{30b}$$

Imposing these conditions on eqns (16) and (28), we get

$$[S_{BB} - S_{BI}S_{II}^{-1}S_{IB} - S_f]\{q_B\} = \{R_B^{(i)}\} - [S_f]\{q_B^{(i)}\} \tag{31a}$$

and

$$q_I = -S_{II}^{-1}S_{IB}q_B. \tag{31b}$$

The displacements of the boundary nodes as well as of the nodes in the interior region are obtained from eqn (31). Then the eqns (30a) and (25) are used to obtain the unknown coefficients in the scattered wave field.

NUMERICAL RESULTS AND DISCUSSION

(a) *Plate bending elements*

The modelling of the interior region by plate bending elements, which interact with the infinite medium (exterior region), is of some interest from the finite element point of view. A number of different plate bending elements have been reported in the finite element literature. The literature in this area is so vast that no attempt will be made here to review it. Among the plate bending elements available, those based on Mindlin's plate theory and selective reduced integration techniques are found to be very effective in modelling the thin as well as thick plate behaviour. Hughes *et al.* (1977) and Pugh *et al.* (1978) studied the performance of quadrilateral plate bending elements in static problems. Their performance in the context of free vibration analysis has been reported by Hinton and Bicanic (1979). Almost all the elements studied in the aforementioned references possess at least one spurious zero-energy mode. It should be noted here that the performance was observed in problems (referred to as "conventional problems" in the sequel) where the plate has a finite span and simple boundary conditions. The prescription of certain boundary conditions may suppress the mechanisms formed by the zero-energy modes. In most applications, these spurious zero-energy modes pose no problem, but occasionally they act up (Hughes *et al.*, 1977; Hughes and Cohen, 1978) when they are weakly coupled to the boundary conditions. The "heterosis" element proposed by Hughes *et al.* (1978) seems to alleviate these shortcomings by having the correct rank and thus possessing no zero-energy mode. Its performance in dynamic problems has not been reported in the literature.

In this study, we consider an infinite plate. However, only the interior region, which is finite, is discretized to get the finite element model. The size of elements is kept within a certain limit in order to ensure that the finite element model transmits the waves effectively. For linear quadrilateral elements, the size is limited to $\frac{1}{8}$ of the minimum wave length of the types of wave being considered. The corresponding "size factor" for quadratic elements is $\frac{1}{4}$. During the experimental stage it was observed that the element aspect ratio (ratio of element size to its thickness) lay within a range of 0.2–1.5. In this range, the elements are known to behave well in conventional problems (no shear locking, etc.). Only four and nine node Lagrange elements and a heterosis element were used in the experiments. The element stiffness was evaluated selectively integrating the bending and shear terms. Results of extensive numerical experiments indicated that all three elements performed well. The nine node Lagrange element and heterosis element exhibited a high level of accuracy and very often, these results hardly differed. The convergence of the four node element was somewhat slow compared to the other two elements, but ultimately converged to the correct results with mesh refinements.

(b) *Scattering by circular cavities*

In order to observe the performance of the plate bending elements in the present context as well as to establish the validity of the proposed technique, we first consider the scattering problem of incident slow flexural waves by a circular cavity in an infinite plate, the angle of incidence being zero. The mesh used for this problem is shown in Fig. 2.

The displacements along the circumference of the cavity are computed for various values of (a) the normalized frequency $\bar{p} = p/p_0$ and (b) the ratio $\bar{a}$ of the radius a of the

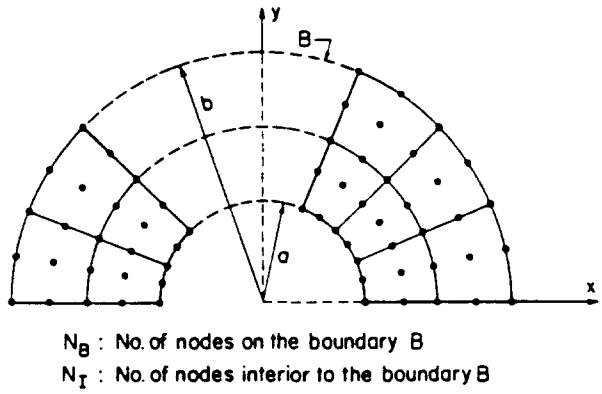

Fig. 2. Finite element mesh.

cavity to the thickness h of the plate. We considered normalized frequencies $\bar{p}$ in the range 0.1–0.9 and $\bar{a}$ from 0.5 to 5.0. The results are found to be in good agreement with the analytical solution. As an illustration, the comparison of a displacement component for a normalized frequency of 0.9 and $\bar{a}$ of 2.0 is shown in Fig. 3. The results of the nine node Lagrange element are not shown on the figure as they are almost identical to those of the

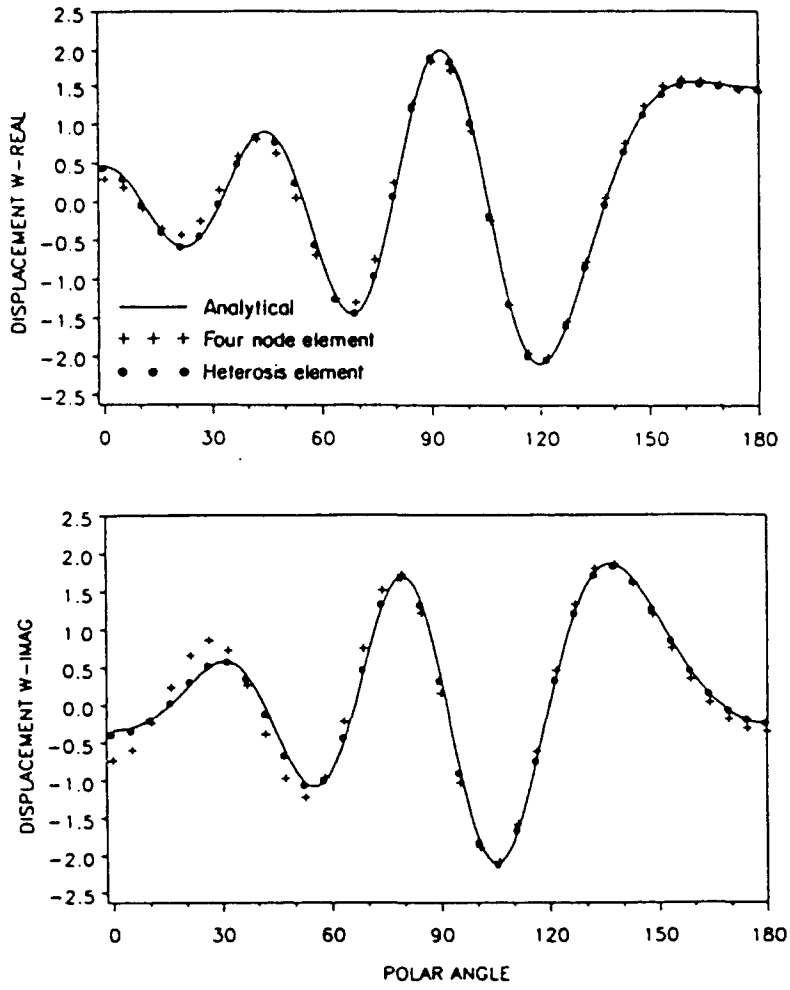

Fig. 3. Displacement along the circumference of the circular cavity ($\bar{p} = 0.9$, $\bar{a} = 2.0$, $\gamma = 0$).

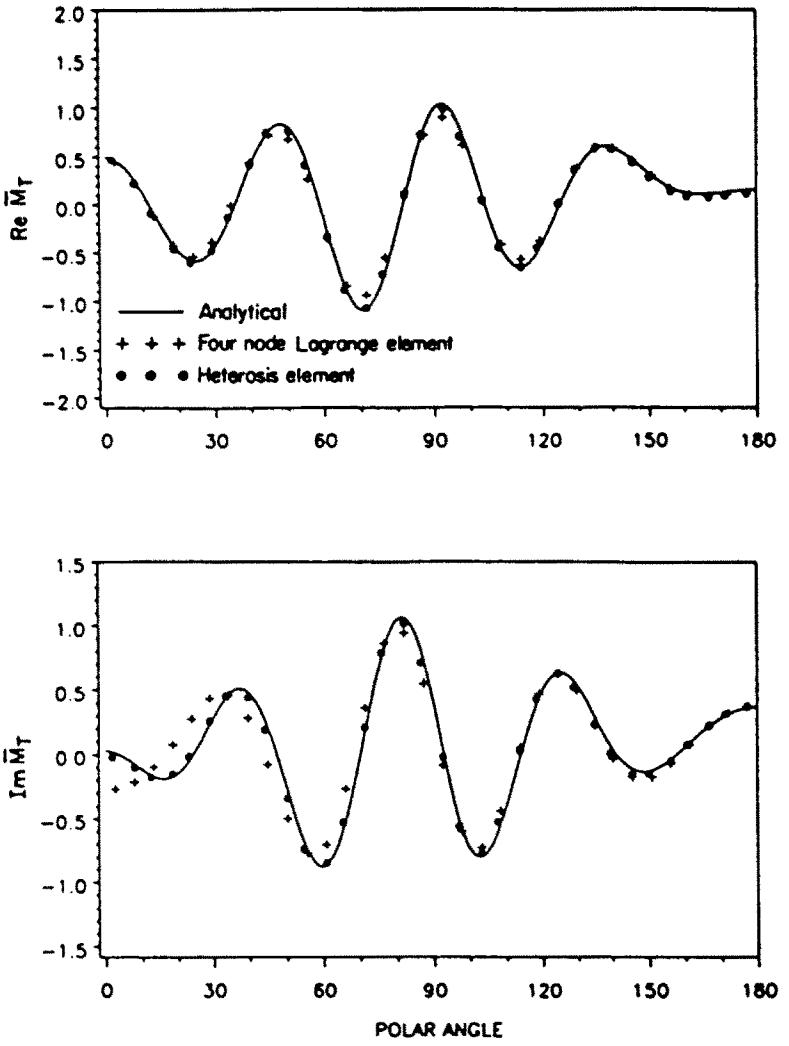

Fig. 4. Variation of tangential moment (parameters are the same as in Fig. 3).

heterosis element. The material properties used in this and other subsequent problems are $\mu = 1.0$, $\nu = 0.3$ and $\rho = 1.0$.

A quantity of general interest in problems involving a cavity is the hoop stress (tangential moment M_T in the present case) along the circumference of the cavity. However, the stress or stress resultant evaluated using the finite element technique at points other than certain Gauss points will be less accurate. The moments are, therefore, computed at those Gauss points that correspond to the shear quadrature and located close to the cavity. These points lie on a circle of radius $1.108\bar{a}$.

Figure 4 shows the normalized moments $\bar{M}_T = M_T/M_0$ so calculated along with the analytical results. The normalization factor M_0 in the above is given by $M_0 = -D\delta_1^2(\sigma_1 - 1)$. The results of the nine node Lagrange element are not shown again as its plot symbols tended to overlap with those of heterosis element. It is seen from Figs 3 and 4 that the nine node Lagrange element and heterosis element are very accurate in modelling the flexural wave scattering phenomenon. The accuracy of the results of the four node element is improved upon refining the mesh.

(c) *Scattering by arbitrary shaped cavities*

Attention is next focussed on the scattering problem of cavities having square and triangular shapes. The radii of their circumscribing circles are $\bar{a}$. The circular cavity con-

sidered previously represents a streamlined scatterer whereas the square and triangular cavities have a blunt nature. The case of multiple scattering by a pair of cavities is also considered where the radii of the cavities are $\bar{a}$ and $\bar{a}$ 2 and their centres are located at a distance $2\bar{a}$. It should be mentioned here that these problems pose no exceptional difficulties to the proposed method. On the other hand, they cannot be solved by analytical means. In these problems, the absolute values of the tangential moments $\bar{M}_T$ are evaluated at Gauss points located close to the circumference of the cavities. (For the square they are on a square with circumscribing circle of radius $1.07\bar{a}$, for the triangle these are on a similar triangle with circumscribing circle of radius $1.08\bar{a}$, and for the two circles the results are around the bigger circle at Gauss points on a concentric circle of radius $1.025\bar{a}$). The normalized values $|\bar{M}_T|$ are then plotted against the polar angle measured at the origin from the positive x-axis in the counterclockwise direction. Only heterosis elements are used for triangular and square cavities. In the case of multiple scattering problems, the finite element model of the interior region tended to be so large that it placed a severe burden on the storage capacity of the computer. Since the bandwidth of the four node element is about half of the nine node element, we alleviated the storage problem by using only the four node elements. Also the results will be presented only for the larger circle in this case.

Figure 5 shows the effect of various $\bar{a}$ values on the tangential moment. With increasing $\bar{a}$ more and more terms of eqn (21) need to be considered to achieve convergence and the fineness of the mesh must be increased accordingly. In this and other subsequent figures, we included the results of circular cavity to facilitate comparison with the results of other cavities. It is seen from Fig. 5 that maximum values occur at the least value of $\bar{a}$. The higher order terms in eqn (21) that become active as $\bar{a}$ increases seem to have the effect of reducing the maximum value but, at the same time, producing more ripples. For the circular cavity, however, the ripples are confined to the first quadrant. This is a "shadow" region to the incoming wave, and the cause of ripples may be partly attributed to the wave that creeps along the boundary of the cavity and disperses in the shadow region. In Fig. 5b, some ripples are observed even in the second quadrant suggesting that the presence of another cavity nearby may extend the shadow region. As anticipated, the corner regions in square and triangular cavities suffer abrupt increase in moments (Fig. 5c, d).

In Fig. 6, we present the results for various normalized frequencies. The value of $\bar{a}$ and angle of incidence γ are fixed at 2.0 and 0°, respectively. The maximum values of the moment seem to occur for the lowest frequency.

Lastly in Fig. 7, results are presented for angles of incidence 0°, 45°, 90°, 135° and 180°. The angles of incidence 135° and 180° are omitted for circular and square cavities as they are similar to 45° and 0°, respectively. Furthermore, different angles of incidence in the case of a circular cavity merely cause a shifting of the curves in the plot. It is seen from Fig. 6 that the maximum values of the moment for different angles of incidence are more or less the same.

CONCLUSION

A hybrid finite element and wave function expansion has been presented to study the scattering of slow flexural waves by arbitrary shaped scatterers in an infinite elastic plate. The scatterer can be either a solid or a cavity. The numerical results presented here agree well with the available analytical results. The advantage of the method is that the near field region containing all inhomogeneities can have quite arbitrary material properties. Also the multiple scattering by a cluster of scatterers can be studied without much difficulty. It is found that the maximum value of the tangential moment around the cavities occurred at the lowest frequency and lowest a/h ratio. It is also found that the maximum value was not much affected by the direction of the incident wave.

Three Mindlin type plate bending elements, namely, four and nine node Lagrange elements and a heterosis element have been used to model the flexural wave scattering phenomenon. Their performance in a similar situation has not been documented previously. It is found that all three elements performed well. The four node element exhibited slow convergence characteristics.

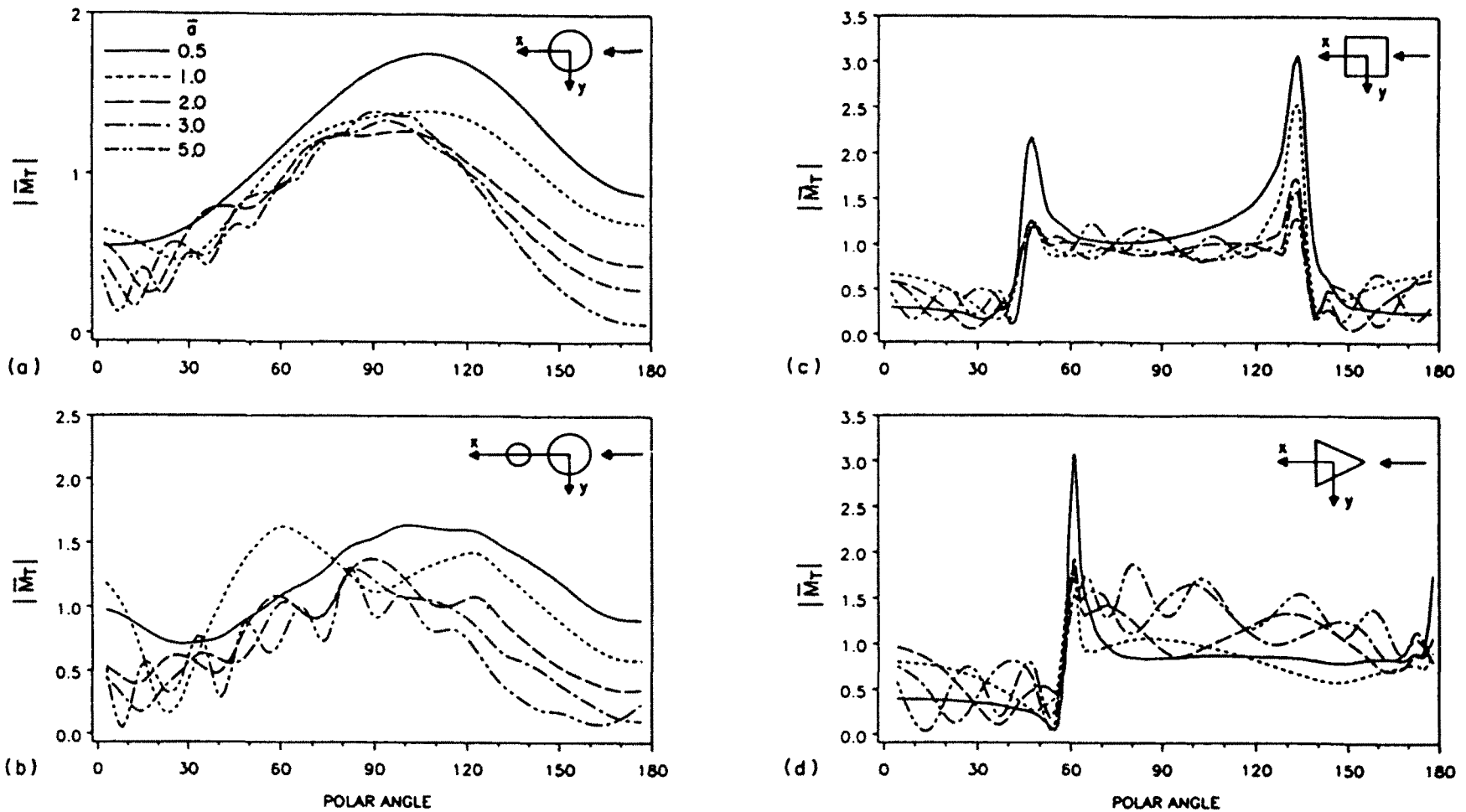

Fig. 5. Effect of $\bar{a}$ on the tangential moment around cavities ($\bar{p} = 0.9, \gamma = 0^\circ$).

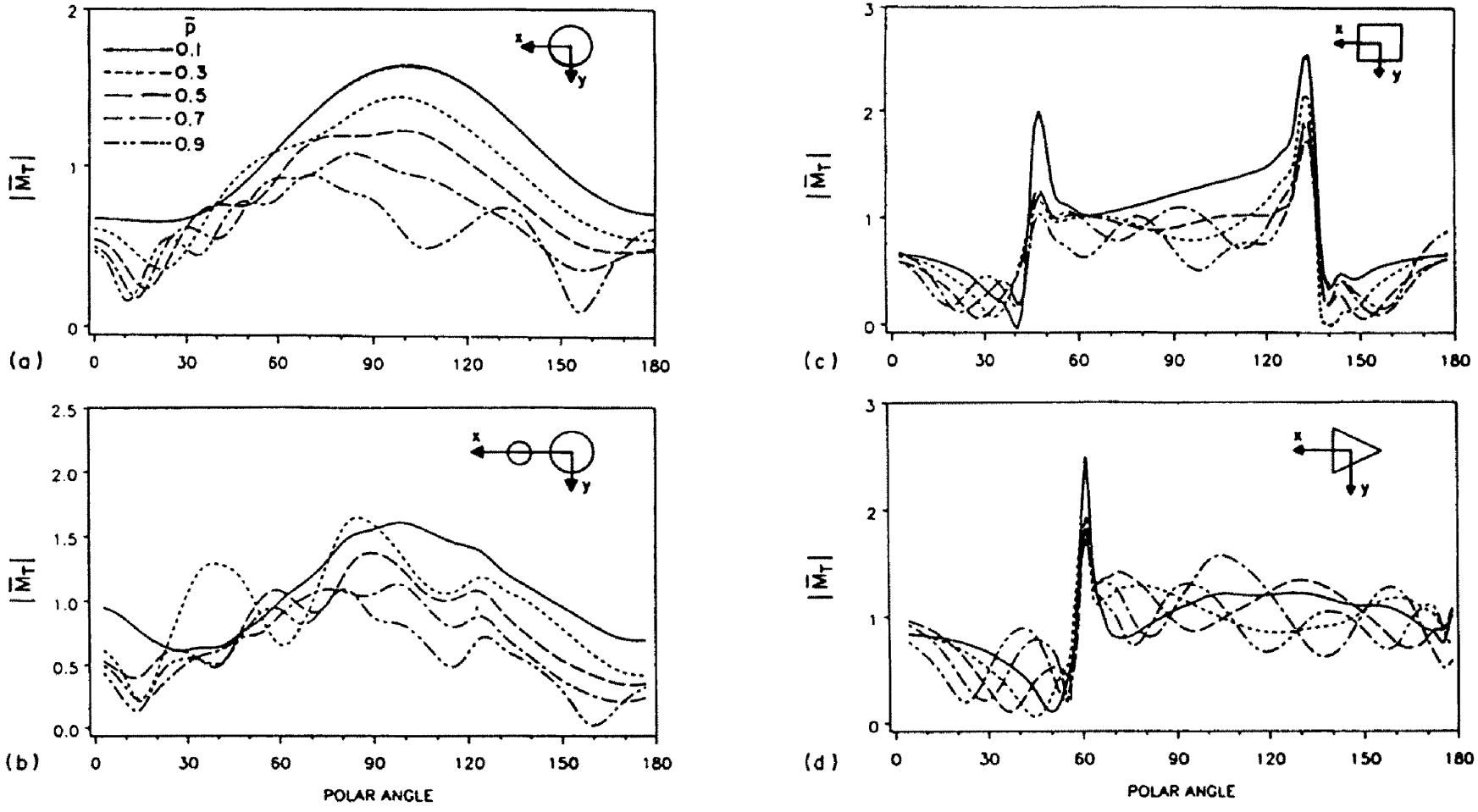

Fig. 6. Effect of frequencies on the tangential moment around cavities ($\bar{a} = 2.0, \gamma = 0°$).

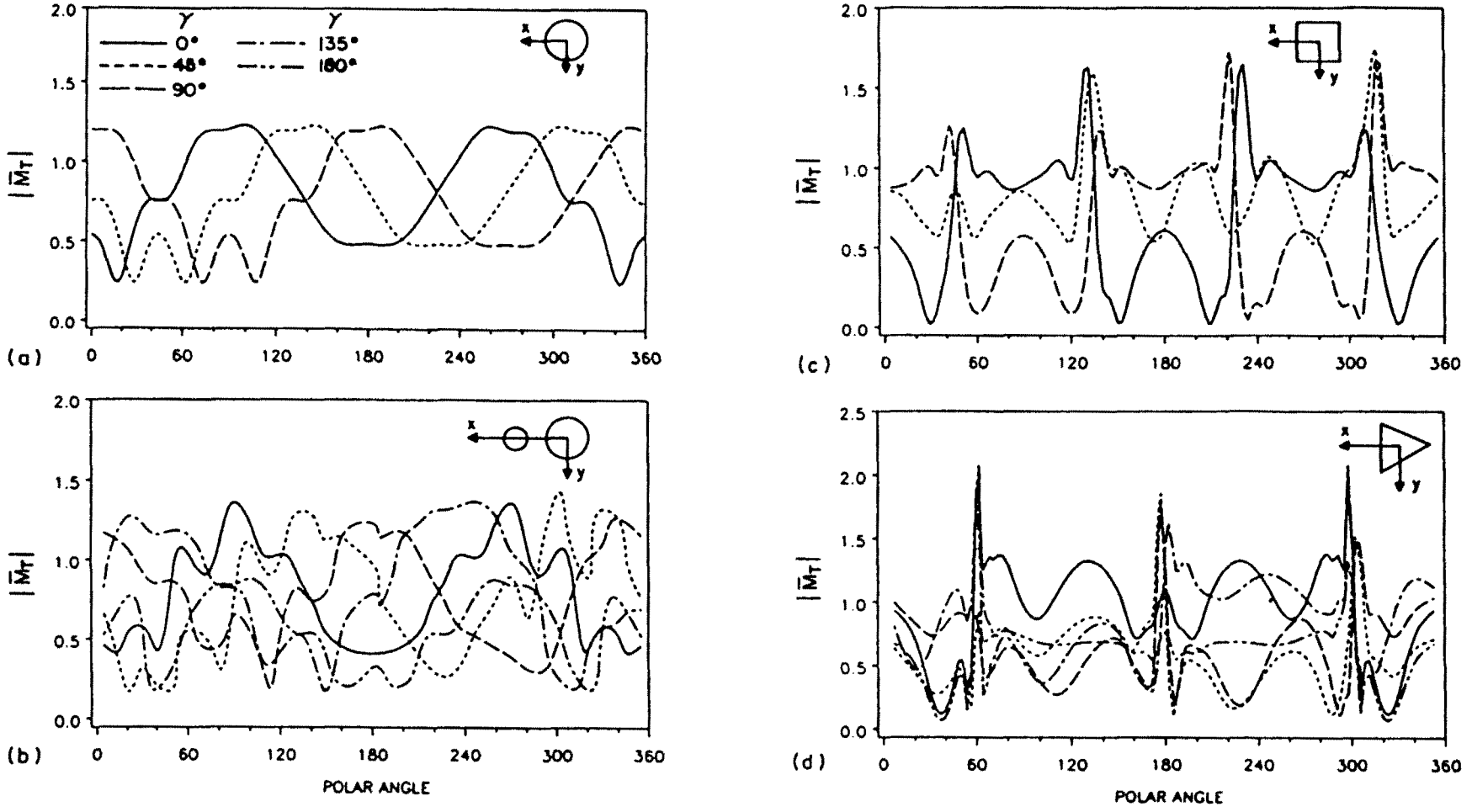

Fig. 7. Effect of incidence angles on tangential moment around cavities ($\bar{\rho} = 0.5$, $\bar{a} = 2.0$).

Acknowledgements—The work here was supported by the Natural Science and Engineering Research Council of Canada (grant No. A-7988). Support was also received from the office of Naval Research (grant No. N00014-86-K-0280; Program Officer, Dr. Y. Rajapakse).

REFERENCES

Abduljabbar, Z., Datta, S. K. and Shah, A. H. (1983). Diffraction of horizontally polarized shear waves by normal edge cracks in a plate. *J. Appl. Phys.* **54**, 461–472.

Chow, Y. K. and Smith, I. M. (1981). Static and periodic infinite solid elements. *Int. J. Numer. Meth. Engng* **17**, 503–526.

Cook, R. D. (1981). *Concepts and Applications of Finite Element Analysis*. John Wiley, New York.

Datta, S. K. and Shah, A. H. (1982). Scattering of SH-waves by embedded cavities. *Wave Motion* **4**, 265–283.

Datta, S. K., Shah, A. H. and Fortunko, C. M. (1982). Diffraction of medium and long wavelength SH-waves by edge cracks. *J. Appl. Phys.* **53**, 2895–2903.

Engquist, B. and Majda, A. (1977). Absorbing boundary conditions for the numerical simulation of waves. *Math. Comput.* **31**, 629–651.

Higden, R. L. (1986). Absorbing boundary conditions for difference approximations to the multi-dimensional wave equation. *Math. Comput.* **47**, 437–459.

Higden, R. L. (1987). Numerical absorbing boundary conditions for the wave equation. *Math. Comput.* **49**, 65–90.

Hinton, E. and Bicanic, N. (1979). A comparison of Lagragian and serendipity Mindlin plate elements for free vibration analysis. *Comput. Struct.* **20**, 483–493.

Hughes, T. J. R., Taylor, R. L. and Kanoknukulchai, N. (1977). A simple and efficient finite element for plate bending. *Int. J. Numer. Meth. Engng* **11**, 1529–1543.

Hughes, T. J. R. and Cohen, M. (1978). The heterosis finite element for plate bending. *Comput. Struct.* **9**, 445–450.

Hughes, T. J. R., Cohen, M. and Haroun, M. (1978). Reduced and selective integration techniques in the finite element analysis of plates. *Nucl. Engng Des.* **46**, 203–222.

Kausel, E., Roesset, J. M. and Waas, G. (1975). Dynamic analysis of footings on layered media. *J. Engng Mech.* **101**, 679–693.

Lee, J. J. and Dasgupta, G. (1984). Interaction of nonlinear interiors with linear infinite domains. In *Numerical Methods for Transient and Coupled Problems* (Edited by R. W. Lewis, E. Hinton, P. Bettess and B. A. Schrefler), pp. 428–438. Pineridge Press, Swansea, U.K.

Lysmer, J. and Kuhlemeyer, R. L. (1969). Finite dynamic model for infinite media. *J. Engng Mech.* **95**, 859–877.

Medina, F. and Taylor, R. L. (1983). Finite element techniques for problems of unbounded domains. *Int. J. Numer. Meth. Engng* **19**, 1209–1226.

Mindlin, R. D. and Deresiewicz, H. (1954). Thickness shear and flexural vibrations of a circular disc. *J. Appl. Phys.* **25**, 1329.

Pao, Y. H. and Chao, C. C. (1964). Diffraction of flexural waves by a cavity in an elastic plate. *AIAA Jnl* **2**, 2004–2010.

Pao, Y. H. and Mow, C. C. (1973). *Diffraction of Elastic Waves and Dynamic Stress Concentrations*. Crane and Russak, New York.

Paskaramoorthy, R., Datta, S. K. and Shah, A. H. (1988). Effect of interface layers on scattering of elastic waves. *ASME J. Appl. Mech.* **55**, 871–878.

Pugh, E. D. L., Hinton, E. and Zienkiewicz, O. C. (1978). A study of quadrilateral plate bending elements with reduced integration. *Int. J. Numer. Meth. Engng* **12**, 1059–1079.

Shah, A. H., Chin, Y. F. and Datta, S. K. (1982a). Elastic waves scattering by surface breaking planar and non-planar cracks. *ASME J. Appl. Mech.* **54**, 761–767.

Shah, A. H., Wong, K. C. and Datta, S. K. (1982b). Diffraction of plane SH-waves in a half-space. *Earthq. Engng Struct. Dyn.* **10**, 519–528.

Shah, A. H., Wong, K. C. and Datta, S. K. (1985). Surface displacements due to elastic wave scattering by buried planar and non-planar cracks. *Wave Motion* **7**, 319–333.

Smith, W. D. (1974). A non-reflecting plane boundary for wave propagation problems. *J. Comp. Phys.* **15**, 492–503.

Ting, L. and Miksis, M. J. (1986). Exact boundary conditions for scattering problems. *J. Acoust. Soc. Am.* **80**, 1825–1827.

APPENDIX

The terms $g_1, g_2, \ldots$ appearing in eqn (23) are as follows

$$g_1 = H_n(\delta_1 r) \tag{A1}$$

$$g_2 = K_n(\delta_2 r) \tag{A2}$$

$$g_{r1} = \bar{\sigma}_1\left[\frac{n}{r}H_n(\delta_1 r) - \delta_1 H_{n+1}(\delta_1 r)\right] \tag{A3}$$

$$g_{r2} = \bar{\sigma}_2\left[\frac{n}{r}K_n(\delta_2 r) - \delta_2 K_{n+1}(\delta_2 r)\right] \tag{A4}$$

$$g_{r3} = \frac{n}{r} K_n(\tilde{\omega} r) \tag{A5}$$

$$g_{t1} = -\tilde{\sigma}_1 \frac{n}{r} H_n(\delta_1 r) \tag{A6}$$

$$g_{t2} = -\tilde{\sigma}_2 \frac{n}{r} K_n(\delta_2 r) \tag{A7}$$

$$g_{t3} = -\left[\frac{n}{r} K_n(\tilde{\omega} r) - \tilde{\omega} K_{n+1}(\tilde{\omega} r)\right]. \tag{A8}$$

The terms Q_{r1}, Q_{r2}, M_{r1}, etc. appearing in eqn (26) are as follows.

$$Q_{r1} = \sigma_1 \left[\frac{n}{r} H_n(\delta_1 r) - \delta_1 H_{n+1}(\delta_1 r)\right] \tag{A9}$$

$$Q_{r2} = \sigma_2 \left[\frac{n}{r} K_n(\delta_2 r) - \delta_2 K_{n+1}(\delta_2 r)\right] \tag{A10}$$

$$Q_{r3} = \frac{n}{r} K_n(\tilde{\omega} r) \tag{A11}$$

$$M_{r1} = \tilde{\sigma}_1 \left[(1-\nu)\frac{n}{r^2}(n-1) - \delta_1^2\right] H_n(\delta_1 r) + (1-\nu)\frac{\delta_1}{r} H_{n+1}(\delta_1 r) \tag{A12}$$

$$M_{r2} = \tilde{\sigma}_2 \left\{\left[(1-\nu)\frac{n}{r^2}(n-1) + \delta_2^2\right] K_n(\delta_2 r) + (1-\nu)\frac{\delta_2}{r} K_{n+1}(\delta_2 r)\right\} \tag{A13}$$

$$M_{r3} = (1-\nu)\left[\frac{n}{r^2}(n-1) K_n(\tilde{\omega} r) - \frac{n\tilde{\omega}}{r} K_{n+1}(\tilde{\omega} r)\right] \tag{A14}$$

$$M_{rt1} = -2\tilde{\sigma}_1 \left[\frac{n}{r^2}(n-1) H_n(\delta_1 r) - \frac{n\delta_1}{r} H_{n+1}(\delta_1 r)\right] \tag{A15}$$

$$M_{rt2} = -2\tilde{\sigma}_2 \left[\frac{n}{r^2}(n-1) K_n(\delta_2 r) - \frac{n}{r}\delta_2 K_{n+1}(\delta_2 r)\right] \tag{A16}$$

$$M_{rt3} = -\left\{\left[\frac{2n}{r^2}(n-1) + \tilde{\omega}^2\right] K_n(\tilde{\omega} r) + \frac{2\tilde{\omega}}{r} K_{n+1}(\tilde{\omega} r)\right\}. \tag{A17}$$